Post-transit time-of-flight currents as a probe of the density of states in hydrogenated amorphous silicon

G. F. Seynhaeve, R. P. Barclay,* and G. J. Adriaenssens
Laboratorium voor Vast-Stof en Hoge-Drukfysica, Katholieke Universiteit Leuven, Celestijnenlaan 200 D, B-3030 Leuven, Belgium

J. M. Marshall
Department of Materials Engineering, University of Wales, University College, Singleton Park, Swansea SA2 8PP, United Kingdom

(Received 23 May 1988; revised manuscript received 14 November 1988)

We use the post-transit photocurrent in a time-of-flight experiment for spectroscopic purposes. It is shown, within the multiple-trapping framework, that the post-transit current is the Laplace transform of the density of states. A simple inversion procedure is suggested and is shown to be quite adequate provided the gap-state distribution does not vary too strongly with energy. The method has been applied to hydrogenated amorphous silicon. Experimental evidence shows that the post-transit photocurrent truly reflects the release out of deeper-lying traps and is not a consequence of nonuniform, time-dependent fields, contact-related properties, or injection phenomena. The measured $\mu_0\tau_d$ are compatible with the deconvoluted density of states. A comparative discussion of our results with other published data obtained with conventional methods like the field-effect, space-charge-limited current, and deep-level transient spectroscopy techniques is given.

I. INTRODUCTION

Measurements of the transient currents due to photoexcited excess carriers have been used extensively in the study of localized band-tail states in amorphous semiconductors. It has been shown that the transport of carriers is delayed by the interaction with these states. Under the assumption that carriers are retarded by capture into localized states and only move in extended states, i.e., by multiple trapping and release events, it is possible to gain information concerning the density and nature of the localized states.

Currently two classes of transient photocurrent experiments can be distinguished. On the one hand, there is the bipolar measurement of the transient photocurrent due to electrons and holes in the gap-cell configuration. This geometry has a low capacitance and ideally the contacts should both have a low resistance. When analyzing coplanar transient photocurrents, the different drift mobilities of electrons and holes, and the densities of trapped and free electrons and holes, along with the recombination, must be taken into account.[1] This technique has been applied to chalcogenide glasses, notably amorphous (*a*-) As_2Se_3, where the current is known to be dominated by hole carriers.[2] The method has also been used on *a*-Si:H,[3] although its validity has been questioned in this case.[4]

On the other hand, unipolar methods can be used to study single-carrier motion. The most common technique is the time-of-flight (TOF) experiment, as described by Spear.[5] Excess carriers of one polarity only are allowed to transit through a sandwichlike sample consisting of a thin-film amorphous semiconductor contained between two electrodes, one of which is semitransparent. Ideally the front contact should be blocking to prevent carrier injection. Carrier accumulation of drifting carriers at the backelectrode can distort the photocurrent; hence, the backelectrode should have a low resistance. To realize this in practice one can either use *p-i-n* devices or Schottky-barrier contacts. Due to the geometry of the configuration, the capacitance C of the sample will be much higher than in the coplanar or gap-cell case. To prevent distortion of the field, the excess charge introduced should be less than CV, where V is the voltage across the sample. Also, the dielectric relaxation time should be larger then the transit time, in order to ensure a uniform field throughout the sample during the drift of the carriers.

The TOF experiment can yield information on the density of states (DOS) in various ways. First, one can deconvolute the pretransit current. By using the simplified thermalization energy approach, as described by Orenstein and Kastner[2] and Tiedje and Rose,[6] an approximate DOS can be obtained from the nonextraction regime. More precise but also more elaborate methods can be used.[7] A comparison between both approaches can be found in Ref. 8. Although deconvolution of the pretransit current has been used successfully on *a*-As_2Se_3, it has not yet been applied to *a*-Si:H for the case of electron transport. This is not surprising, since it is difficult to obtain a pretransit current over an appreciable time scale. Furthermore, one has to be cautious of effects which can distort the transient photocurrent. For example, distortions due to contact potentials should be considered. Given that the drift mobility of holes is about 1000 times lower than that of electrons at room temperature, the method can, however, be used to study the valence-band-tail states in *a*-Si:H.[9]

Second, one can gain information from the dependence of the drift mobility on temperature and electric field.[10] However, since the activation energy of the drift mobility is only slightly field dependent, the DOS can only be determined over a small energy range (0.08–0.15 eV) from the conduction-band mobility edge.

Third, one can focus on the post-transit photocurrent. It is the purpose of this paper to describe the theoretical and experimental procedure which will allow the use of TOF post-transit photocurrents as a spectroscopic tool. A simple inversion procedure will be described and its limit of validity discussed. While the proportionality between post-transit current and the trap distribution was recognized before (see, e.g., Ref. 6), no practical application has so far been attempted.

Various effects which could influence the post-transit photocurrent analysis (PTPA) will be critically assessed. The method will then be applied to *a*-Si:H, since all prerequisites can best be met with this amorphous semiconductor.

II. EXPERIMENTAL PROCEDURE AND DETAILS

The standard TOF experimental arrangement was used to measure the electron transient photocurrents. As a digitizer, an IWATSU TS-8123 oscilloscope was used with a 100-MHz 1-MΩ input amplifier. The repetition rate of the nitrogen dye laser ($\lambda = 540$ nm) was kept low; at least 30 s elapsed between light pulses. Usually ten shots were averaged to increase the 9-bit resolution of the digitizer at longer times. Before each series of light flashes, the dark-current response of the sample to the field pulse was recorded. The dark current was then subtracted from the photocurrent before averaging took place. The noise due to the nitrogen laser was reduced to a minimum by proper screening of electromagnetic interference. The intensity of the light pulse was reduced until the shape of the current trace became independent of intensity to ensure the absence of space-charge distortion.

The time interval between the application of the field and the firing of the laser was kept constant at 7 μs. By measuring at successive time decades and concurrently changing the resistance over which the current was measured, a time span from 5 ns to 5 s could be obtained. Since the HP-214B pulse generator used for the field pulses has a maximum pulse length of 10 ms, dc biases were applied when studying the response over longer times. The influence of the dc field on the current trace will be discussed in Sec. III C. A typical current trace obtained in this way is shown in Fig. 1. The photocurrents could be measured reliably up to 1% of the dark-current level. The photocurrent can roughly be divided into three time regions. First there is the pretransit region (region I) when virtually no carriers have left the sample. Region II marks the arrival at the backelectrode of the bulk of the free-carrier distribution. At the moment when the mean of the free-charge-carrier distribution arrives at the end of the sample, the current has al-

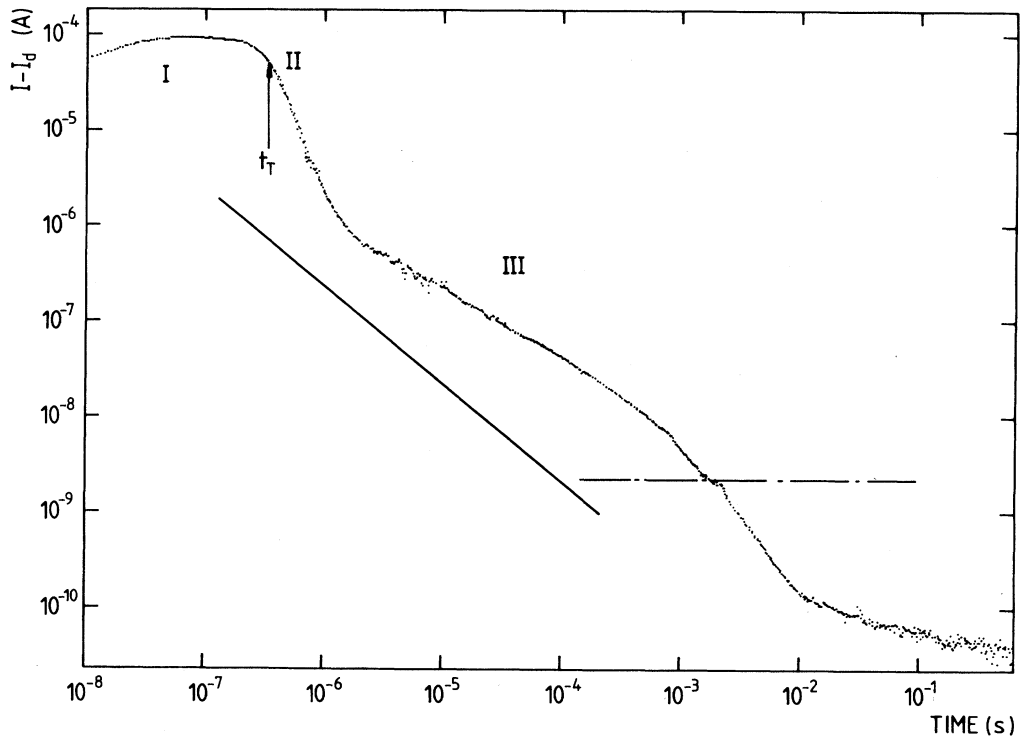

FIG. 1. Typical experimental electron-current trace obtained with a bias voltage of 0.6 V over a 5-μm undoped *a*-Si:H film. The arrow marks the transit time. Collected charge was 36 pC. A t^{-1} law is drawn for reference (solid line) and the dc dark current level is also indicated (dash-dot line).

ready dropped by a factor of 2 compared with the extrapolated pretransit current. Finally, in region III the deeply trapped charge is released and extracted.

The 5-μm-thick a-Si:H samples used for electron post-transit measurements were deposited at the Studiecentrum voor Kernenergie (SCK), Mol, Belgium, on Corning 7059 glass substrates precoated with Cr. 50-Å-thick (2×3)-mm^2 Cr contacts were evaporated on top of the film. Cr contacts were chosen for their well-documented contact properties.[11] In this configuration, the internal field is equivalent to that of two back-to-back Schottky barriers. When the illuminated electrode has a negative polarity, the first barrier is reverse biased, hence blocking, while the second is forward biased, i.e., low resistant. This is in agreement with contact requirements for the TOF experiment. Use of a Cr/a-Si:H/n^+-type device could eventually lower the resistance at the backelectrode even more. The ESR spin density was measured to be smaller than 10^{16} cm^{-3}. Hydrogen effusion measurements showed that the film contained about 6 at. % hydrogen. By fitting the collected charge as a function of applied field to a Hecht curve, we obtained a $\mu_0\tau_d$ product of $\approx 5\times10^{-7}$ cm^2 V^{-1}, where μ_0 is the microscopic mobility and τ_d the deep trapping lifetime. In the Hecht formula a fitting parameter was added to the applied field to correct for the contact potential. The $\mu_0\tau_d$ value obtained is comparable to values obtained by others[12,13] on low-defect-density material.

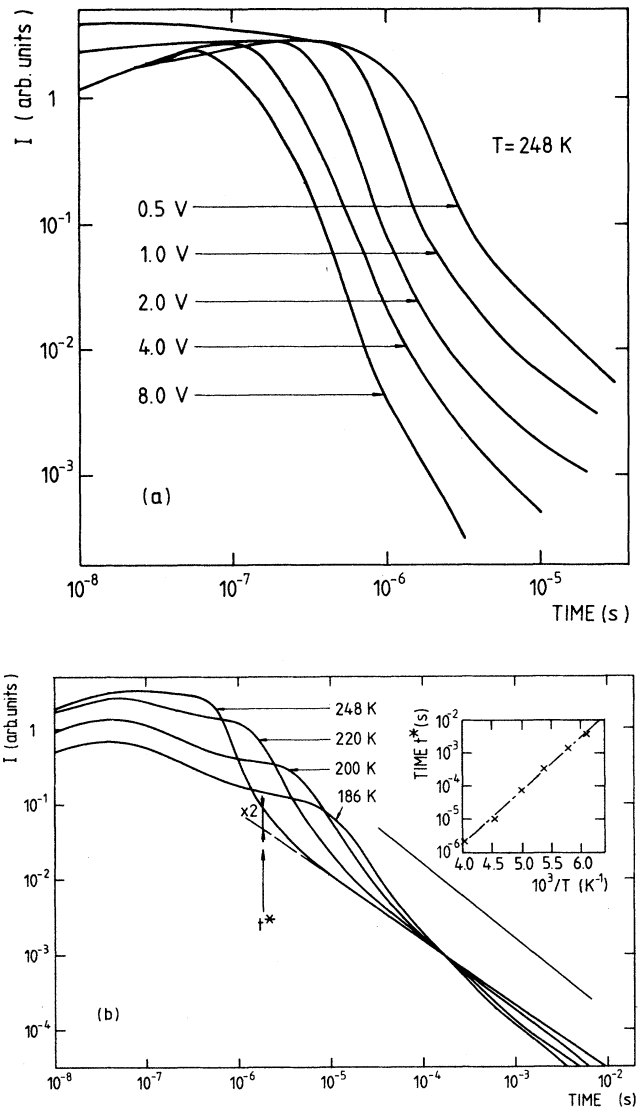

FIG. 2. (a) The field dependence of the photocurrent. The curves have been normalized to the same initial current which scales proportional to F. (b) Temperature dependence of the photocurrent at a bias of 1 V. A t^{-1} law is drawn for reference. The point marked t^* showed a thermally activated behavior, of which the Arrhenius plot is reproduced in the inset.

In Fig. 2(a), experimental electron-current traces for different electric fields are shown. The curves have been normalized to the same initial current. After the transit, the current falls quite steeply before changing to a slower decay (region III), which can be measured up to times of order 1 s. It is found that the normalized post-transit photocurrents are lower by a factor of roughly 4 when the field is doubled. Figure 2(b) shows the temperature dependence of the current trace.

If the temperature is lowered, the changeover from region II to III shifts to longer times. The point t^* marked in Fig. 2(b) corresponds to the time when the extrapolation of the region III current to short times is half of the actual photocurrent. It is used as a measure for the changeover in the decay and shows a thermally activated behavior, as shown in the inset of Fig. 2(b). There is also a slight temperature dependence of the slope in the third time regime. For lowering temperature the slope approaches -1, while at higher temperatures it is shallower (slope > -1). In the next section a procedure will be described to deconvolute the current in region III to a DOS below the conduction-band tail.

III. ANALYSIS OF POST-TRANSIT TIME CURRENTS

A. Theoretical outline

If one assumes that the transport of carriers in an amorphous semiconductor is retarded by multiple trapping into and release from discrete gap levels, a set of rate equations which describes this model in the small-signal case can readily be written down:[14]

$$\frac{\partial n_0}{\partial t}+\mu_0 F\frac{\partial n_0}{\partial x}=-\sum_{i=1}^{m}\frac{\partial n_i}{\partial t}+\frac{Q_0}{e}\delta(x)\delta(t)\ ,$$
$$\frac{\partial n_i}{\partial t}=\omega_i n_0-r_i n_i,\quad i=1,\cdots,m\ . \tag{1}$$

Here F is the externally applied field, μ_0 is the microscopic mobility, and the n_i are the densities of carriers in different energy levels. Index 0 refers to the transport band and m to the number of levels. Q_0 is the amount of excess charge, assumed positive, which takes part in the transport process (each carrier has a charge e). The density of states enters the equations via the capture and

release coefficients ω_i and r_i:

$$\omega_i=\sigma\bar{v}N_i, \quad r_i=\nu_0 e^{-E_i/kT} .$$

σ is the capture cross section, $\bar{v}$ is the thermal velocity of the carriers, E_i is the energy position of the ith level, and we assume a positive energy direction towards the Fermi level. The origin is taken at the appropriate mobility edge and the levels are ΔE apart. N_i is the number of states at the energy E_i, which is equal to $g(E_i)\Delta E$, where g is the density-of-states function. The release constant depends on the attempt-to-escape frequency ν_0 and the temperature T. Capture and release constants are coupled through detailed balance, which requires that

$$\nu_0=\sigma\bar{v}g(0)kT .$$

$g(0)$ is the density of states at the mobility edge. Assuming ν_0 to be temperature independent (hence $\sigma\bar{v}\sim 1/kT$) we obtain

$$\omega_i=\nu_0\frac{g(E_i)\Delta E}{g(0)kT}=\nu_0\bar{g}(E_i)\frac{\Delta E}{kT} , \tag{2}$$

where we have introduced a normalized DOS $\bar{g}(E)$.

The solution of Eqs. (1) can readily be obtained by Laplace transformation. The transformed current is then[15]

$$\mathcal{L}_s(I(t))=Q_0\left[\frac{1-e^{-a(s)t_0}}{a(s)t_0}\right] ,$$

$$a(s)=s\left[1+\sum_{i=1}^{m}\frac{\omega_i}{s+r_i}\right] , \tag{3}$$

$$t_0=L/\mu_0 F ,$$

where L is the length of the sample. Since the inversion of this expression for the Laplace-transformed current is not physically transparent, we will consider two extreme cases. First, if $a(s)t_0$ is large, we obtain the expression for the current before the extraction at the backelectrode starts (region I):

$$\mathcal{L}_s(I_<(t))=Q_0/a(s)t_0 . \tag{4}$$

This can be inverted to

$$I_<(t)=(Q_0/t_0)\sum_{i=0}^{m}A_i e^{-s_i t} . \tag{5}$$

The $-s_i$ are the $(m+1)$ roots of the equation $a(s)=0$. The A_i are then given by

$$A_i=\left[1+\sum_{j=1}^{m}\frac{\omega_j r_j}{(r_j-s_i)^2}\right]^{-1}, \quad i=0,\ldots,m . \tag{6}$$

On the other hand, when $a(s)t_0$ is small, one finds

$$I_>(t)\simeq(Q_0t_0/2)\sum_{i=1}^{m}\omega_i r_i e^{-r_i t} . \tag{7}$$

The time span in which either Eq. (5) or Eq. (7) should be a valid approximation can be found by considering the movement of the first moment $\langle x(t)\rangle$ of the spatial free-carrier distribution in a semi-infinite model. During the period when $0<\langle x(t)\rangle<L$ virtually no carriers will have left the sample. So Eq. (5) will be a good approximation. Once $\langle x(t)\rangle>L$, most of the carriers will exit at the backelectrode. In that case Eq. (7) should be used.

It can be shown that $\langle x(t)\rangle=L$ is a good definition for the transit time t_T, provided the spatial free-carrier distribution is sufficiently symmetric.[16] For times after t_T the photocurrent will be increasingly dominated by the release of the carriers out of deep traps and not by the transport of carriers through the sample.

For the case of a continuous distribution, Eq. (7) can be reformulated to

$$I_>(t)=(Q_0t_0\nu_0/2)\int_{r_1}^{r_2}\bar{g}(r)e^{-rt}dr , \tag{8}$$

where r_1 corresponds to the release rate from the lowest energy and r_2 is equal to ν_0. In practice we can approximate r_1 by zero and r_2 by infinity. In this way the normalized DOS and the post-transit photocurrent are linked via a Laplace transform:

$$I_>(t)=(Q_0t_0\nu_0/2)\mathcal{L}_t(\bar{g}(r)) . \tag{9}$$

So the density of states is found by Laplace inversion of $I_>(t)$, which, for experimental current traces, has to be done numerically.

Fortunately, the inversion can be simplified by approximating the exponential waiting-time distribution for release out of a trap an energy E deep: $r(E)e^{-r(E)t}$, by a δ function $\delta(rt-1)$. This means that instead of having an *average* release time $r(E)^{-1}$, *all* trapped carriers at an energy E become free at $r(E)^{-1}$. We then obtain

$$tI_>(t)=(Q_0t_0\nu_0/2)\bar{g}(E) , \quad E=kT\ln(\nu_0 t) , \tag{10}$$

where the energy and time are related by the thermalization-energy expression. A different derivation of Eq. (10) for the ambipolar transport in gap cells may be found in Ref. 17. The result does of course also confirm the earlier Tiedje and Rose[6] post-transit expression, but with a proportionality constant which now follows directly from the multiple-trapping rate equations.

The energy range over which Eq. (10) is valid is limited to the post-transit regime, i.e., when the photocurrent is dominated by extraction and not by the transport of carriers. Since carriers which are trapped at the same energy but at different places in the sample, e.g., at the front contact or just at the backelectrode, have a difference in arrival time of t_T at the most, it is indicated to use post-transit currents only from $2t_T$ on.

Below it will be shown that Eq. (10) is a satisfactory approximation for the DOS, at least for amorphous semiconductors, which are expected to exhibit a slowly varying DOS as a function of energy.

B. Numerical simulations

To study the influence of the DOS on the transient photocurrent we have taken two different approaches. First, the validity of Eq. (10) has been checked by assuming various model densities of states, then calculating the post-transit current via Eq. (7) and finally inverting it via Eq. (10). Second, to study the field and temperature

dependence of the transient photocurrent, a numerical, backward-Euler, implicit integration scheme as first used by Main in Ref. 1 has been implemented to integrate the set of differential equations (1).

In Figs. 3(a) and 3(b) a comparison is made between an input DOS and the inversion via Eq. (10) after calculating the current via Eq. (7). Two examples of distributions have been considered. In both cases an exponential function with $T_0=300$ K has been used to describe the band-tail states. The first model distribution that we consider is one in which a Gaussian feature has been added [Fig. 3(a)]:

$$\bar{g}(E)=g_0 e^{-E/kT_0}+g_1\exp\left[-\frac{1}{2}\left[\frac{E-E_0}{\sigma}\right]^2\right], \quad \bar{g}(0)=1 . \tag{11}$$

This is to verify how reliably Eq. (10) can reproduce distinct levels in the gap.

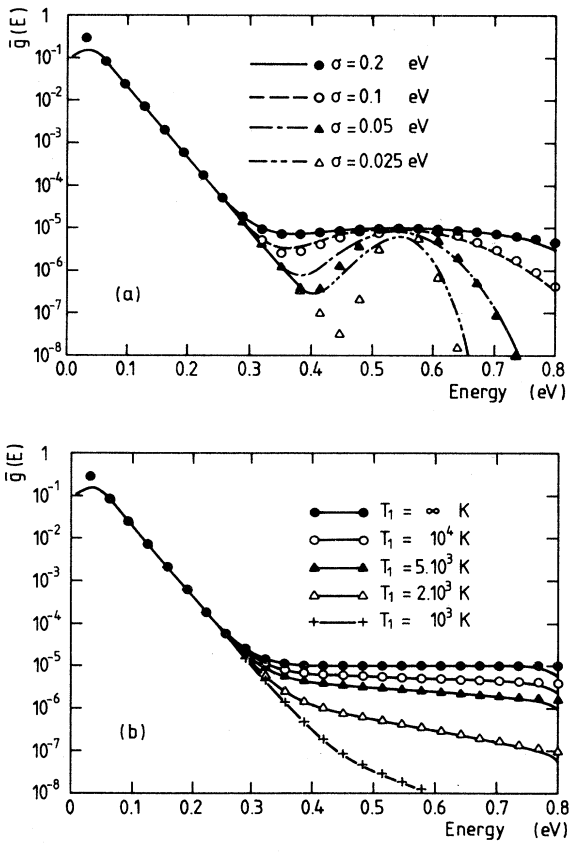

FIG. 3. (a) Comparison of input DOS (symbols) and output DOS (lines) obtained via Eq. (10) for an exponential tail with a Gaussian feature. Parameters used are $T=T_0=300$ K, $\nu_0=10^{12}$ Hz, $t_0=10^{-9}$ s. Different values of the variance σ have been taken, while g_1 and E_0 were kept constant at 10^{-5} and 0.51 eV, respectively. (b) Comparison of input DOS (symbols) and output DOS (lines) obtained via Eq. (10) for linear combination of two exponentials. The characteristic temperature of the first exponential was kept constant at 300 K, while the second has been varied as indicated. Other parameters as in (a).

By varying the width of the Gaussian distribution we find that deviations become considerable for sharp distributions. This behavior can be illustrated by considering a discrete level:

$$\ln[\bar{g}(E)]=\ln[G\delta(E-E_0)] . \tag{12}$$

Via Eqs. (7) and (10) this transforms to

$$\ln[\bar{g}(E)]=(E-E_0)/kT-e^{(E-E_0)/kT}+\ln(G) , \tag{13}$$

which represents a distribution which is "smeared out" around the input energy level E_0. The full width at e^{-1} of the maximum is $\simeq 3kT$. This is the amount of broadening expected in any spectroscopic method which relies on the thermalization-energy approach.

Another interesting model density is described by the sum of two exponentials and is the second distribution that we consider [Fig. 3(b)]. This DOS is useful because the result of the inversion procedure can be calculated analytically. For any monotonically decreasing DOS which can be described by a linear combination of exponentials

$$\bar{g}(E)=\sum_{i=0}^{n} B_i e^{-E/kT_i} ,$$
$$\sum_{i=0}^{n} B_i=1 , \tag{14}$$
$$B_i>0 \text{ and } T_i>0 ,$$

Eq. (10) will yield

$$\bar{g}(E)=\sum_{i=0}^{n} B_i\Gamma(1+T/T_i)e^{-E/kT} . \tag{15}$$

When the temperature T is smaller than the smallest T_i, $0.83\le\Gamma(1+T/T_i)\le 1$. The result is then only slightly different from the input DOS.

To study the influence of the electric field on the full current trace, we performed some numerical simulations on the DOS described by Eq. (11). The parameters used for the Gaussian feature were $\sigma=0.06$ eV and $g_1=7.75\times10^{-6}$. The results are shown in Fig. 4. The currents have been normalized to the same initial current in the same manner as the experimental curves are normalized. Note that although the pretransit current is proportional to the electric field, the post-transit current is inversely proportional to it. This is immediately clear from Eqs. (5) and (7). Experimentally it is thus advantageous to use low electric fields.

However, if the field becomes too low, the simulated current traces start to coalesce and region I shows an exponential decay. Also, the apparent transit time becomes field independent. For a purely exponential tail, such a behavior is not observed in the simulated current traces, so it must be a consequence of trapping into the Gaussian feature of the distribution. This can be understood by considering the total capture rate into the Gaussian distribution:

$$\tau^{-1}=(\nu_0/kT)\int \bar{g}_{\text{Gauss}}(E)dE ; \tag{16}$$

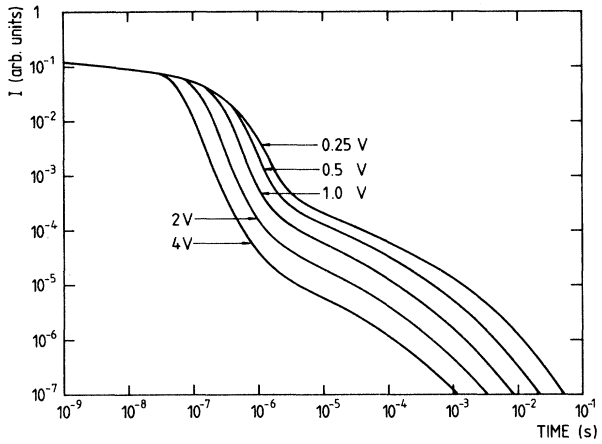

FIG. 4. Full current trace obtained by numerical integration of Eq. (1). A DOS described by Eq. (11) has been used with $g_1=7.75\times10^{-7}$ and $\sigma=0.06$ eV. The length of the sample was fixed at 5×10^{-4} cm while the voltage was changed. All other parameters as explained in the text.

when the capture time τ becomes shorter than the free-carrier transit time t_0, carriers will preferentially be trapped into the Gaussian feature, rather than exit the sample. By introducing an effective lifetime τ_e we can mix the two competing processes, namely extraction, at the backelectrode and trapping into Gaussian states:

$$\tau_e^{-1}=\tau^{-1}+t_0^{-1} . \tag{17}$$

The turnover point in the full current trace is not simply proportional to τ_e, because the observed lifetime is enhanced by multiple trapping and release events. However, it illustrates the dependence on the electric field. For high fields or low-defect-density material ($\tau\gg t_0$), τ_e varies with electric field, while for low fields or high-defect-density material ($\tau\ll t_0$), τ will dominate in Eq. (17) and so there will be no field dependence. Such behavior has also been observed experimentally[18] and has been called "deep trapping."

It should, however, be emphasized that whether or not the trapping is deep is strictly dependent on the time scale of the experiment. For example, in our simulations no carriers are lost due to recombination, so the integral of the current up to infinite time always yields Q_0, i.e., the total generated charge, independent of the field applied. However, if we integrate the current only up to, say, 1 μs, as is usually done experimentally, the collected charge versus field fits a Hecht curve:

$$Q(F)=Q_0(\tau_d/t_0)(1-e^{-\tau_d/t_0}) , \tag{18}$$

where τ_d is in good agreement with the τ defined in Eq. (16). This illustrates that τ_d, the deep trapping lifetime, is dependent on the time range considered.

It should also be pointed out that when τ is smaller than t_0, Eq. (7) is no longer valid, since it was derived under the assumption that $a(s)t_0\ll1$. Experimentally, a transit time scaling with the electric field must be observed before post-transit photocurrents can be inverted reliably with Eq. (10). This puts a lower limit on the applied field.

C. Analysis and discussion of the experimental results

In order to calculate the normalized DOS as a function of energy through Eq. (10), one needs values for the attempt-to-escape frequency ν_0, the free-transit time t_0, the charge Q_0 involved in the multiple-trapping process, and the temperature T.

An estimate for the attempt-to-escape frequency was obtained via the temperature-activation plot of the point marked t^* in Fig. 2(b). A fit of the data to the thermalization-energy expression yields a value of 0.32 eV for the energy of the level associated with t^*, and an attempt-to-escape frequency of $(1.0-1.6)\times10^{12}$ Hz. Due to the smooth decay at longer times, it was not possible to estimate ν_0 and E_A, the activation energy, for other features in the gap. A value of 10^{12} Hz has therefore been used for all energies below 0.32 eV. This value of ν_0 is in order-of-magnitude agreement with the trapping parameters obtained from charge collection[19] and indicates that the deep trapping is into neutral centers with a capture cross section of $\approx10^{-15}$ cm^2.

A value of 10 cm^2 V^{-1} s^{-1} was used for the free mobility. In Ref. 10 a value of 20 cm^2 V^{-1} s^{-1} was determined as a good estimate, but the analysis is based on the transit time of the fastest free carriers, which is roughly half that of the mean free carriers. Other measurements based on the transit time of the mean free carriers also yield values for the mobility of 10 ± 5 cm^2 V^{-1} s^{-1}.[20]

The charge Q_0 was determined by integrating the current trace. Taking a value of 3×10^{21} cm^{-3} eV^{-1} for the value of the DOS at the mobility edge $g(0)$ (Ref. 21) finally yields the absolute number of states. In Fig. 5 the DOS's obtained for different current traces are shown.

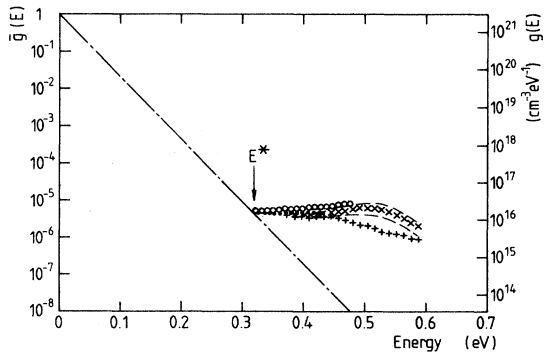

FIG. 5. Compilation of the DOS from different current traces obtained on two codeposited samples. The crosses (+) refer to results obtained at room temperature for one particular sample. All other results are from another sample but are taken at different temperatures: 300 K (×) (the current trace from Fig. 1 was used), 243 K (○), and 220 K (●) [current traces shown in Fig. 2(b)]. The dashed lines give the outer bounds for the DOS after repeated measurements. An exponential tail (not measured) with $T_0=300$ K is also shown. The parameters used were $\nu_0=10^{12}$ Hz and $\mu_0=10$ cm^2 V^{-1} s^{-1}. E^* is the energy corresponding to the point t^* in the current trace of Fig. 2(b).

Comparing the results at room temperature yields an uncertainty of about a factor of 2 for the normalized DOS. The absolute number of states will scale with the choices of ν_0, μ_0, and $g(0)$, according to Eq. (10). As one can see, the DOS is more or less constant with a value of about 10^{16} cm^{-3} eV^{-1}. If we compare the experimental results with the simulations of Fig. 3(a), we see that there is no necessity for a further refinement of the inversion formula (10).

The experimentally determined DOS can also be correlated with the measured $\mu_0\tau_d$ product. Taking as an estimate for the number of deep states the measured density minus the extrapolated exponential tail, one obtains $\simeq 2\times10^{-6}$ eV for the normalized number of states. Substitution of this into an expression analogous to Eq. (16) gives a value of 1.5×10^{-7} cm^2 V^{-1} for $\mu_0\tau_d$, where we have used the previously mentioned values for ν_0 and μ_0. This is in reasonable agreement with the experimental value, obtained by fitting the collected charge versus field with a Hecht curve, as described in Sec. II, of 5×10^{-7} cm^2 V^{-1}. Note that the correlation of the number of deeper states to the $\mu_0\tau_d$ product as described here is independent of the values used for ν_0 and μ_0, since these cancel out [this can easily be verified by substitution of Eq. (10) into Eq. (16)].

The analysis of long-time current decays as presented here will only be useful insofar as the multiple trapping and release events dominate the transport process. In what follows, we will therefore identify other processes which might be relevant to the long-time behavior of the TOF transients, and try to estimate their importance and influence.

Since we measure the photocurrent over an extended period of time, dielectric relaxation of the field due to the thermally excited carriers will occur. Generally the time taken by the field to relax in a semiconductor is $t_d=\rho\epsilon$, ρ being the resistivity and ϵ the permittivity of the material. For a-Si:H, $\rho\epsilon$ is about 10–40 ms at room temperature. Experimentally, the influence of dielectric relaxation can be seen when comparing photocurrent traces obtained with either pulsed or constantly applied voltage, as represented in Fig. 6. When a pulsed voltage is used, the field remains uniform for times $\leq t_d$; on the other hand, the field due to a constant applied voltage is fully relaxed. Clearly, the field distribution has a profound influence on the pretransit current. We also see that the transit shifts to longer times in the latter case. However, the post-transit current exhibits the same overall decay. This illustrates the fact that the post-transit is not affected by a time-dependent relaxing field.

The influence of dielectric relaxation on the photocurrent can also be illustrated by simulating the photocurrent for various stationary fields which represent different stages of relaxation. Since little is known on the shape of the relaxed field in an amorphous-silicon Schottky barrier, reasonable estimates have to be made. It is known[11] that the material first deposited on the substrate has more defects than the bulk of the material. Hence, the depletion width and the barrier height will be reduced, resulting in a strongly asymmetric internal field.

Experimentally determined barrier profiles can be described by an exponentially decaying field for distances less than 1 μm from the barrier. In the absence of extrinsic doping, the internal field is determined by the density of states. Under the assumption of a constant DOS with a value g, one obtains[22] for the static barrier profile

$$F(x)=F_0e^{-x/\lambda_D},\quad \lambda_D=(\epsilon/ge^2)^{1/2}\ , \tag{19}$$

where x, the distance from the interface, is 0 at the barrier and positive into the sample and the field is directed towards the barrier. λ_D is the Debye screening length (see also Ref. 23). If we neglect the low resistive backcontact, and assume that the form of the electric field under reverse bias is similar to that of the static barrier, we can write

$$F(x)=F_0e^{-x/\lambda},\quad \Delta V=\int_0^L F(x)dx\ , \tag{20}$$

where ΔV is the potential difference across the sample, and λ a parameter which describes the relaxation of the field. When the field is applied for times smaller than t_d, λ will be large, resulting in a near uniform field. When the field is applied for times smaller then t_d, λ will start to diminish, resulting in a field which drops within a small distance from the blocking electrode. It should be stressed that the assumed shape of the electric field given by Eq. (20) is only for illustrative purposes and is not derived from the analysis of the reverse-biased Schottky barrier.

In Fig. 7 the results are depicted for various values of λ and F_0 while ΔV is kept constant at 1 V. As one can see, the shape of the pretransit current drastically changes and the transit time shifts to longer times with decreasing λ. The post-transit current keeps its same overall shape except when t_0 becomes larger than the deep trapping lifetime. This insensitivity to the shape of the internal field is easy to understand when one considers that the post-transit current is related directly to release from

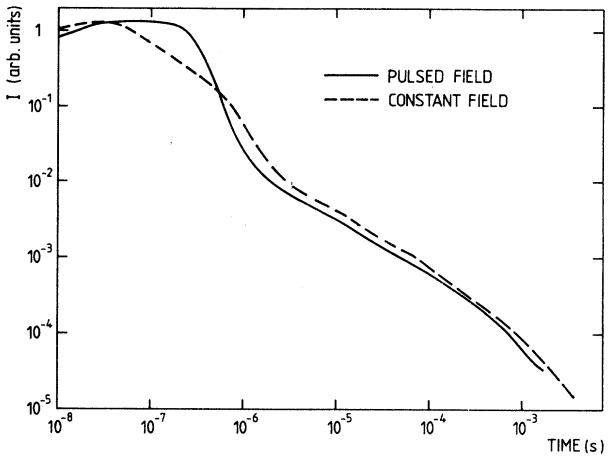

FIG. 6. Comparison of experimental current traces for a pulsed and a constant applied field. A negative bias on the top electrode of 0.6 V has been used in both cases. Temperature was 298 K. Curves have been slightly offset vertically for ease of comparison. The dielectric relaxation time is about 10–20 ms.

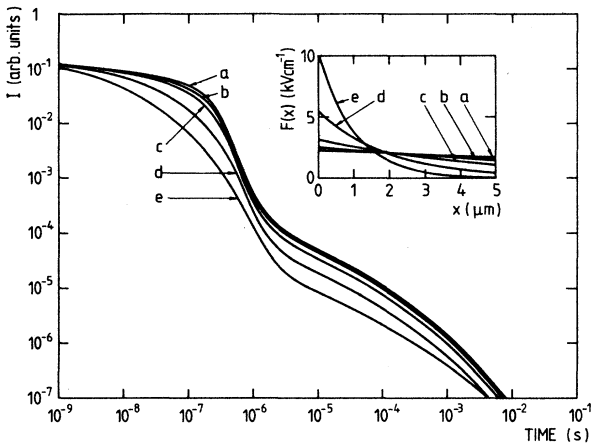

FIG. 7. Calculated photocurrent traces for nonuniform fields. The DOS used is the same as for Fig. 4 and the voltage difference ΔV was kept constant at 1 V.

traps. Since the release time t_r of the traps which are observed in the post-transit photocurrent is larger then the transit time t_T, a carrier which detraps at t_r will only suffer a relatively small delay of at the most t_T before it arrives at the backelectrode. Whether this t_T is small (uniform field) or large (relaxed field) does not matter as long as one only uses the photocurrent after $2t_T$, as stated earlier.

Another process which may distort the post-transit current is electron-hole recombination. However, if the recombination lifetime of the electrons is significantly smaller than the free-electron transit time, this would mean that electrons recombine with holes rather than become extracted at the backelectrode. Such small electron-hole recombination times are in contradiction with the observed field dependence of the transit time. In the fully relaxed field case there could possibly be a region where the drift velocity is very low and where enhanced recombination could occur. Such low fields, as can be shown in simulations with a nonuniform field, result in very long transit times. Since in the experiments with constant applied field a transit time is still well defined and found to shift with the applied field (although not directly proportional to the inverse of it), we may conclude that an appreciable field must exist throughout the whole sample even under constant field conditions, and that recombination is not a problem.

The interpretation up to now has not taken into account the fact that states situated around the Fermi level are occupied, since they are in thermal equilibrium with the band. In principle one would expect a sharp drop in the photocurrent when states just above the Fermi level are emptied. However, once the thermalization energy of the excess carriers approaches the dark-current Fermi level, the occupation of the states with thermal electrons has the effect of reducing the capture rate for excess electrons. Consequently, the lifetime of the excess electrons increases, which leads to an increase in charge density and hence current (photoconductive gain). So, at long times the photocurrent minus the dark current will tend to level off, as can be seen in the experimental current trace of Fig. 1, before dropping to the final equilibrium dark level. The magnitude of this effect will increase with increasing excess charge, and can be reduced by using as low an excitation level as possible. The effect is comparable with the "trap saturation," as it is sometimes found in coplanar configuration photocurrents.[24] It is obvious that the simple analysis via Eq. (10) is no longer applicable, since no account has been taken of degeneracy or the equilibrium occupation of the states.

We also have to be aware of the possible influence of surface effects. If there is an increased DOS at the metal-semiconductor interface, this could preferentially trap the photogenerated charge and act as a charge reservoir. By using deeply penetrating light of $\lambda \simeq 640$ nm, which is absorbed within $\simeq 1$ μm, the majority of the carriers are created beyond the surface region. We do not observe any change in post-transit current behavior with deeply penetrating light, indicating that the surface region does not play a significant role.

Perhaps the clearest evidence that the post-transit photocurrent is directly related to the DOS is the observation of light-induced defects. When illuminating a sample with unfiltered light from a 250-W tungsten lamp, an increase is observed in the DOS between 0.4 and 0.6 eV. Simultaneously, a decrease in the $\mu_0\tau_d$ product is measured. However, a detailed description of the experimental relation between the DOS and $\mu_0\tau_d$ is beyond the scope of this article and will be published elsewhere.

IV. COMPARISON WITH OTHER METHODS AND CONCLUSIONS

In the previous paragraphs we have explored the theoretical and practical limits of the spectroscopic use of the post-transit photocurrent analysis (PTPA). The DOS obtained in this way is internally consistent with the measured $\mu_0\tau_d$ product.

It is also found that the magnitude of the DOS and the energy scale is dependent on the attempt-to-escape frequency and the free mobility. Although we have determined ν_0 to be $\approx 10^{12}$ Hz out of the activated behavior of one single point in the DOS, it is still controversial what the energy and/or temperature dependence of ν_0 is.[25]

Before we compare our results with those obtained through other, more established techniques, it is worthwhile emphasizing that the DOS of undoped a-Si:H can exhibit deviations from sample to sample when measured with the same method. Despite these variations, well-known methods such as the space-charge-limited currents technique (SCLC) give more or less the same behavior for the DOS within an order of magnitude. However, if one compares different techniques, the results differ more than can be expected on the basis of sample-to-sample variation.

In Fig. 8 a comparison is made of four different techniques: field effect, SCLC, deep-level transient spectroscopy (DLTS), and PTPA. Representative averages have been taken where possible. Apparently the highest DOS is predicted by field-effect measurements, while the lowest is given by DLTS; SCLC and PTPA both fall somewhere

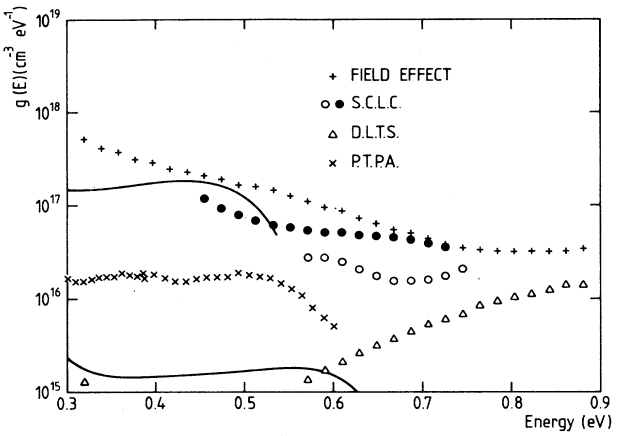

FIG. 8. Comparison of different DOS obtained by various techniques [+, field effect (Ref. 26); *, DLTS (Ref. 27); ●, SCLC (Ref. 28); ○ SCLC (Ref. 29); ×, PTPA]. The solid lines indicate the result obtained by PTPA for $\nu_0 = 10^{11}$ Hz (upper curve) and $\nu_0 = 10^{13}$ Hz (lower curve).

in between. The magnitude of the localized-state distribution below the band tail is comparable for PTPA and SCLC, although the shape is somewhat different. Increasing or decreasing ν_0 by an order of magnitude would decrease or increase the PTPA DOS by as much and change the energy range as shown in Fig. 8 (solid lines). Changing μ_0 will result in a proportional offset of the PTPA DOS. This could bring the results more in agreement with the other methods, but is, of course, in contradiction with the measured ν_0 and the accepted value of μ_0.

The reason for the differences between, e.g., the DLTS and field-effect results, is still not completely understood, although possible reasons have been discussed.[30] A magnitude of more than 10^{17} cm^{-3} eV^{-1}, as obtained by the field-effect technique is, however, difficult to reconcile with the deep trapping lifetimes usually measured in undoped material. Such a value for the DOS would result in too small deep trapping lifetimes, with the numbers assumed here for ν_0 and μ_0. Surface states are normally considered to be the origin of the large field-effect DOS.[30] To enlarge the energy range in field-effect spectroscopy one normally dopes the sample. In DLTS as well it is necessary to dope samples in order to form a Schottky barrier. However, doping is known to change the DOS.[31]

The occurrence of gap states in *a*-Si:H is attributed to the existence of dangling bonds. A compilation of energy levels in undoped *a*-Si:H of the neutral (D^0) and charged states (D^-,D^+) of the defect obtained by different methods has been given in Ref. 32. The results fall into two different groups: one which situates the D^- at an energy of 0.8–0.9 eV below E_c and another which puts the D^- level at 0.5–0.6 eV below E_c. This duality does persist in more recently published results involving new experimental techniques such as the transient-photomodulation-spectroscopy study of Stoddart *et al.*,[33] which points to the lower values, or the below-gap modulated photocurrents used by Abe *et al.*,[34] which support the 0.5-eV assignment.

Our results cover the higher of those two energy ranges. Since the DOS we measure there can be reversibly moved up and down by light soaking and annealing, we may assume that we are seeing D^- centers. Their distribution does not show a marked maximum in the 0.5–0.6-eV area (although individual samples can exhibit some structure); the overall impression is more of an essentially constant density of states. If such distribution were part of an even broader band of D^- states, say up to ~ 1.0 eV, then the observation of D^- states at either 0.6 or 0.9 eV could depend on whether the experiment being performed is more sensitive (for whatever reason) to states in the upper or in the lower part of the band.

In summary, post-transit photocurrents in a TOF experiment can conveniently be used for spectroscopic purposes on undoped samples in situations where the use of other techniques is prohibited. Changes in the DOS induced by light soaking can be measured by PTPA. Various simulations and experiments have assured us of the validity of the theoretical approximations and eliminated the occurrence of possible experimental side effects which may have distorted the photocurrent.

ACKNOWLEDGMENTS

Samples were kindly prepared and supplied by Professor P. Nagels, J. Smeets, and M. Van Rooy at the Studiecentrum voor Kernenergie, Mol (Belgium). Financial support for this research has been obtained from the Belgian "Interuniversitair Instituut voor Kernwetenschappen."

*Permanent address: Department of Materials Engineering, University of Wales, Singleton Park, Swansea SA2 8PP, U.K.

[1]C. Main, R. Russell, J. Berkin, and J. M. Marshall, Philos. Mag. Lett. **55**, 189 (1987).
[2]J. Orenstein and M. Kastner, Phys. Rev. Lett. **46**, 1421 (1981).
[3]J. Hvam and M. Brodsky, Phys. Rev. Lett. **46**, 371 (1981).
[4]R. A. Street, Phys. Rev. B **32**, 3910 (1985).
[5]W. E. Spear, J. Non-Cryst. Solids **1**, 197 (1969).
[6]T. Tiedje and A. Rose, Solid State Commun. **37**, 49 (1981).
[7]H. Michiel, J. M. Marshall, and G. J. Adriaenssens, Philos. Mag. B **48**, 187 (1983).
[8]J. M. Marshall, R. P. Barclay, C. Main, and C. Dunn, Philos. Mag. B **52**, 997 (1985).
[9]J. M. Marshall, R. A. Street, M. J. Thompson, and W. B. Jackson, Philos. Mag. B **57**, 387 (1988).
[10]J. M. Marshall, R. A. Street, and M. J. Thompson, Philos. Mag. B **54**, 51 (1986).
[11]R. A. Street, Phys. Rev. B **27**, 4924 (1983).

[12]R. A. Street, J. Zesch, and M. J. Thompson, Appl. Phys. Lett. **43**, 672 (1983).
[13]W. E. Spear, H. L. Steemers, and H. Mannsperger, Philos. Mag. B **48**, L49 (1983).
[14]F. W. Schmidlin, Phys. Rev. B **16**, (1977).
[15]W. D. Lakin, L. Marks, and J. Noolandi, Phys. Rev. B **15**, 5837 (1977).
[16]G. Seynhaeve, G. J. Adriaenssens, H. Michiel, and H. Overhof, Philos. Mag. B **58**, 421 (1988).
[17]J. G. Simmons and M. C. Tamm, Phys. Rev. B **7**, 3709 (1973).
[18]H. Steemers, W. E. Spear, and P. G. LeComber, Philos. Mag. B **47**, L83 (1983).
[19]R. A. Street, Philos. Mag. B **49**, L15 (1984).
[20]A. C. Hourd and W. E. Spear, Philos. Mag. B **51**, L13 (1985).
[21]W. B. Jackson, C. C. Tsai, and S. M. Kelso, J. Non-Cryst. Solids, **77&78**, 281 (1985).
[22]I. Solomon, T. Dietl, and D. Kaplan, J. Phys. (Paris) **39**, 1241 (1978).
[23]K. H. Henisch, *Semiconductor Contacts* (Clarendon, Oxford, 1984), Sec. 2.1, p. 42.
[24]E. A. Schiff, Phys. Rev. B **24**, 6189 (1981).
[25]H. Okushi, Philos. Mag. B **52**, 33 (1985); D. V. Lang, J. D. Cohen, J. P. Harbison, M. C. Chen, and A. M. Sergent, J. Non-Cryst. Solids **66**, 217 (1984).
[26]R. E. Schropp, Ph.D. thesis, University of Groningen, 1987.
[27]J. D. Cohen, D. V. Lang, and J. P. Harbison, Phys. Rev. Lett. **45**, 197 (1980).
[28]K. D. MacKenzie, P. G. LeComber, and W. E. Spear, Philos. Mag. B **46**, 377 (1982).
[29]W. denBoer, J. Phys. (Paris) Colloq. **42**, C4-451 (1981).
[30]H. Fritzsche, J. Non-Cryst. Solids **77&78**, 273 (1985).
[31]C. R. Wronski, B. Abeles, T. Tiedje, and G. D. Cody, Solid State Commun. **44**, 1423 (1982).
[32]P. G. LeComber and W. E. Spear, Philos. Mag. B **53**, L1 (1986).
[33]H. A. Stoddart, Z. Vardeny, and J. Tauc, Phys. Rev. B **38**, 1362 (1988).
[34]K. Abe, H. Okamoto, Y. Nitta, Y. Tsutsumi, K. Hattori, and Y. Hamakawa, Philos. Mag. B **58**, 171 (1988).